RSC Advances

ROYAL SOCIETY OF CHEMISTRY

www.rsc.org/advances

Supercapacitor based on longitudinal unzipping of multi-walled carbon nanotubes for high temperature application

P. Sivaraman[a,b], Sarada P. Mishra[a], Dharshana D. Potphode[a], Avinash P. Thakur[a], K. Shashidhara[a], Asit B. Samui[a] and Arup R. Bhattacharyya[b*]

[a] Naval Materials Research Laboratory, Shil Badlapur Road, Anand Nagar, Ambernath-421506, Thane, Maharashtra, India

[b] Department of Metallurgical Engineering and Materials Science, Indian Institute of Technology Bombay, Mumbai-400076, India

Abstract

Multi-walled carbon nanotubes (MWCNTs) were partially unzipped longitudinally by the chemical method. Unzipped multi-walled carbon nanotubes (UZ-MWCNTs) were characterized by transmission electron microscopic analysis, X-ray diffraction and Raman spectroscopic analyses. UZ-MWCNTs were utilized for the electrode preparation and the electrodes were used in the fabrication of supercapacitor. At room temperature, UZ-MWCNTs based supercapacitor showed specific capacitance of ~41 Fg^{-1}, while pristine MWCNTs based supercapacitor exhibited 22 Fg^{-1} at the scan rate of 25 mVs^{-1}. The increase in specific capacitance was attributed to an increase in effective specific surface area of UZ-MWCNTs due to partial unzipping. UZ-MWCNTs based supercapacitor exhibited an increase in specific capacitance with increase in temperature. It showed specific capacitance of ~74 Fg^{-1} at 100 °C at the scan rate of 25 mVs^{-1}, while the pristine MWCNTs based supercapacitor did not show any appreciable change in specific capacitance as a function of temperature. UZ-MWCNTs exhibited three-fold increase in specific capacitance as compared to pristine MWCNTs at 100 °C. Impedance spectroscopic analysis of the supercapacitors revealed that the UZ-MWCNTs based supercapacitor exhibited higher internal resistance and lower leakage resistance than pristine MWCNTs based supercapacitor. Continuous 'charge-

discharge' cycling behaviour indicated that UZ-MWCNTs based supercapacitor exhibited lesser stability during initial cycles even though it depicted higher specific capacitance as compared to pristine MWCNTs based supercapacitor.

Keywords: multi-walled carbon nanotubes, unzipping, specific capacitance, impedance spectra, supercapacitor

* Author to whom all the correspondence should be addressed:

Email: arupranjan@iitb.ac.in, Tel. No: +91-22-2576-7634, Fax: +91-22-2572 6975

Introduction

Supercapacitors also termed as electrochemical capacitors, have attracted much attention to the researchers in recent years. It exhibit several advantages viz., high power density, long cycle life over batteries and high energy density over conventional capacitors [1,2]. Supercapacitors bridge the gap between conventional dielectric capacitors and batteries [3,4]. Hence, supercapacitors find applications in electric vehicles, uninterrupted power supplies, telecommunication systems, load cranes and forklifts industrial power management [5,6].

Carbon nanotubes (CNTs) exhibit unique properties and could be found suitable in applications viz, supercapacitors, batteries and fuel cells [7,8]. CNTs have been utilized as electrode material in the supercapacitor due to their high surface area, excellent electrical conductivity, high corrosion resistance and unique pore structure [9-12]. CNTs could store charges through electric double layer formation at the interface between the electrode and the electrolytes and the storage process has been shown to be electrostatic in nature. Both single-walled carbon nanotubes (SWCNTs) and multi-walled carbon nanotubes (MWCNTs) have been used as electrode material in the supercapacitors. SWCNTs exhibited high specific capacitance due to their high specific surface area [13-16]. In contrast, MWCNTs showed lower specific capacitance due to the multiple concentric cylinders associated with their morphology and slower diffusivity of the ions into inner tubes [17-20]. A considerable amount of research has been addressed to improve the specific capacitance of MWCNTs. In this context, surface modification of MWCNTs was carried out to enhance the specific conductance. Frackowaik et al. reported that the specific capacitance of MWCNTs was increased from 80 to 135 Fg^{-1}, while treating MWCNTs with 69% nitric acid [8, 9]. Moreover, activation of MWCNTs by KOH could increase the surface area from 430 to 1035

m^2g^{-1} and consequently, the specific capacitance was increased significantly [8]. Activation of MWCNTs by KOH at 800 °C and/or ammoxidation at 350 °C has resulted in the incorporation of nitrogen containing groups onto the surface of CNTs, which subsequently could improve the specific capacitance of CNTs through pseudo-capacitive behaviour [20]. Oxidation of MWCNTs by electrochemical method has increased the surface area by opening the tips of the MWCNTs, which might facilitate the diffusion of the ions into the inner tubes. Moreover, surface characteristic of MWCNTs might change from hydrophobic to hydrophilic type, which could increase the wettability of the electrolytes. This in turn could lead to the improvement in specific capacitance of MWCNTs from 32.7 to 335.2 Fg^{-1}. Further, chemical oxidation by an extremely aggressive oxidizing agent such as mixed acid; viz., H_2SO_4/HNO_3 might introduce hydrophilic carboxyl groups on the CNTs surface and has improved the wetting characteristic of CNTs in the presence of aqueous electrolytes and could enhance the specific capacitance of MWCNTs to a large extent [22]. The surface treatment of MWCNTs with NH_3 plasma has also increased the wettability of the CNTs and consequently, increased the specific capacitance from 38.7 to 207.3 Fg^{-1} [24]. The specific capacitance of MWCNTs could be increased with the incorporation of functional groups on MWCNTs surface. However, the modification of MWCNTs surface leads to a decrease in electrical conductivity and hence, a balance between hydrophilicity and electrical conductivity is necessary to achieve higher specific capacitance [23]. The above studies strongly suggest that specific capacitance of MWCNTs could be increased either by increasing the active surface area, which should be accessible to electrolyte ions or by introducing surface functional groups to nanotubes, which might undergo redox reaction and subsequently exhibit pseudo-capacitance.

Recently, unzipping of the MWCNTs to yield ribbon of graphene sheets both by chemical methods and electrochemical methods has been reported [25-35]. A majority of the studies reported for unzipped MWCNTs (UZ-MWCNTs) based supercapacitors have utilized aqueous electrolytes [26-32]. Even though MWCNTs based supercapacitors utilizing aqueous electrolytes exhibit high power density due to the high electronic conductivity and readily accessible surface area. However, the energy density is a concern for these supercapacitors. The energy density of a supercapacitor could be improved either by increasing the specific capacitance of the electrode material and/or by using a non-aqueous electrolyte. Since, the upper voltage of non-aqueous supercapacitor could be ~ 3 V, the energy storage ($E=1/2\ CV^2$) could be increased by 9 times as compared to an aqueous electrolyte based supercapacitor with an upper voltage of ~1V.

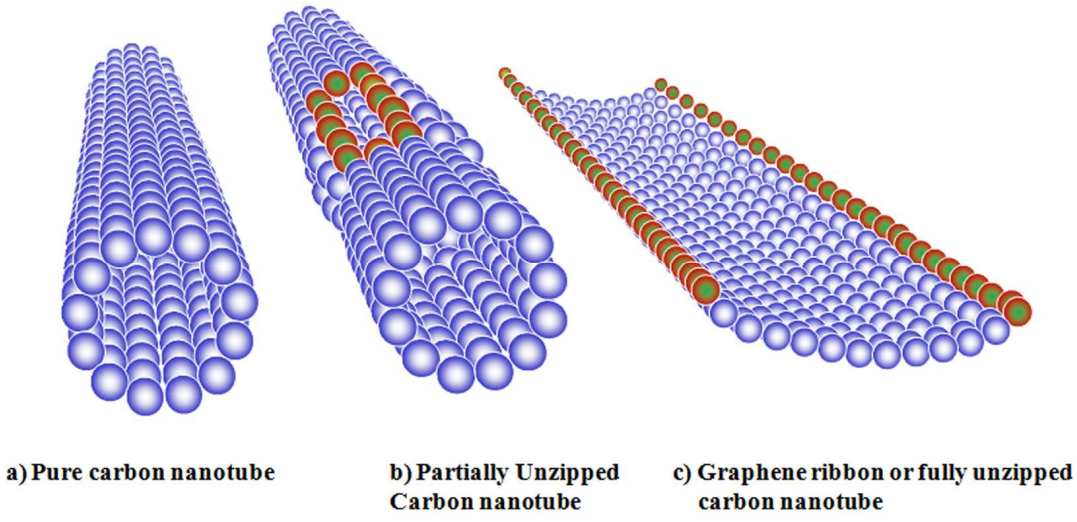

Figure 1: A schematic of longitudinal unzipping of carbon nanotubes

In this present study, supercapacitor of high energy density based on MWCNTs is reported by increasing the specific capacitance of MWCNTs utilizing partially unzipped MWNTs, in a non-aqueous electrolyte. A schematic of the unzipped MWCNTs is shown in figure 1. As the MWCNTs were partially unzipped, the diffusion mechanism of the ions and

the resistance associated with 'charge-discharge' process could be different from that of pristine MWCNTs based supercapacitor. An attempt has been made in this investigation to compare the electrochemical behaviour of pristine MWCNTs and UZ-MWCNTs based supercapacitors in non-aqueous electrolyte at different temperatures.

Experimental

Materials

MWCNTs used in this study were obtained from Nanocyl SA, Belgium (Grade: NC 3100; thin purified multi-walled carbon nanotubes, purity ≥ 95%, D=9.5 nm and L= 1.5 μm as per manufacturer specifications). PTFE suspension was purchased from Hindustan Fluorocarbons Ltd, India. Carbon paper was obtained from Toray, Japan. Sulphuric acid (98%), Hydrogen peroxide (30%), hydrazine hydrate (64%), potassium permanganate (99%) and propylene carbonate (PC) were purchased from Merck, India and used without further purification. Tetra ethylene ammonium tetrafluoroborate ($TEABF_4$) salt was obtained from Alfa Aeser.

Synthesis of Unzipped MWCNTs

Synthesis of UZ-MWCNTs was carried out following the procedure provided elsewhere [25, 26]. In a typical recipe, 2.5 g of MWCNTs were dispersed in 200 mL of concentrated H_2SO_4 for 2 h and then 500 wt% of $KMnO_4$ was added to it, at room temperature following which the reaction mixture was stirred at 70 °C for 1 h. The reaction was quenched by adding small amount of H_2O_2 and ice cold water. The reaction mixture was filtered using a PTFE membrane and then washed thoroughly with distilled water several times. Reduction of oxidized MWCNTs was carried out by treating with hydrazine hydrate

and ammonia solution for 24 h. UZ-MWCNTs was subsequently washed thoroughly and then dried at 60 °C for 24 h.

Electrode preparation

10 mg of MWCNTs or UZ-MWCNTs was mixed with poly (tetrafluoro ethylene) (PTFE) suspension (0.5 mg of PTFE) in a mortar and pestle to yield a paste. The paste was applied uniformly on the carbon paper of size 2 cm x 2 cm and dried at room temperature for 24 h.

Unit cell fabrication

The unit cell of the supercapacitor was prepared by using two electrodes separated by a capacitor grade separator paper. The assembly was dried at 60 °C for 24 h in a vacuum oven attached to the Mbraun Glove box. The assembly was sealed with plastic coated aluminium foil after addition of electrolyte (1M $TEABF_4$ in propylene carbonate; PC). Sealing of the assembly was carried out inside the glove box, which was kept under nitrogen atmosphere. The sealed unit cells were kept in between two heating plates attached with temperature controller and clamped tightly to carry out electrochemical characterization at high temperature.

Characterizations

Transmission electron microscopic (TEM) analysis of MWCNTs and UZ-MWCNTs was carried out using a transmission electron microscope (CM 200, Philips; operated at 200 kV). Dilute suspension of MWCNTs or UZ-MWCNTs was sonicated in isopropyl alcohol

and then a drop of the respective suspension was casted on a copper grid for TEM investigation.

Raman spectroscopic analysis was performed using a HR 800 micro–Raman spectrometer (Jobin Yovon, France) on powder samples with incident laser excitation wavelength of 514 nm.

X-ray diffraction (XRD) analysis of the powder samples was carried out using Philips X'Pert X-ray diffractometer.

Supercapacitors were characterized by two electrode method (unit cell) at different temperatures. Cyclic voltammetry, galvanostatic 'charge-discharge' measurement and electrochemical impedance spectroscopic investigations were carried out using Ecochimie Autolab PGSTAT30.

Electrochemical impedance spectroscopic measurements of the supercapacitors were carried out in the frequency range of 1 MHz to 5 mHz at the cell potential of 1.25 V.

Results and Discussion

a. Physical characterization of the UZ-MWCNTs

Figure 2 shows the morphology of the pristine and unzipped MWCNTs. SEM and TEM micrographs corresponding to pristine MWCNTs (Figure 2a and 2d) exhibit smooth surface containing concentric cylinders of entangled carbon nanotubes. On the contrary, TEM micrographs of UZ-MWCNTs (Figure 2b, 2c) show highly irregular tube boundaries along with few graphene type layers containing entangled concentric nanotubes of MWCNTs. Moreover, SEM micrographs of UZ-MWCNTs (Figure 2e, 2f) indicate that the average width or diameter of the UZ-MWCNTs is larger than pristine MWCNTs due to partial

longitudinally opened carbon nanotubes. These observations are in agreement with that reported by Kosynkin et al. [25] and Wang et al. [26].

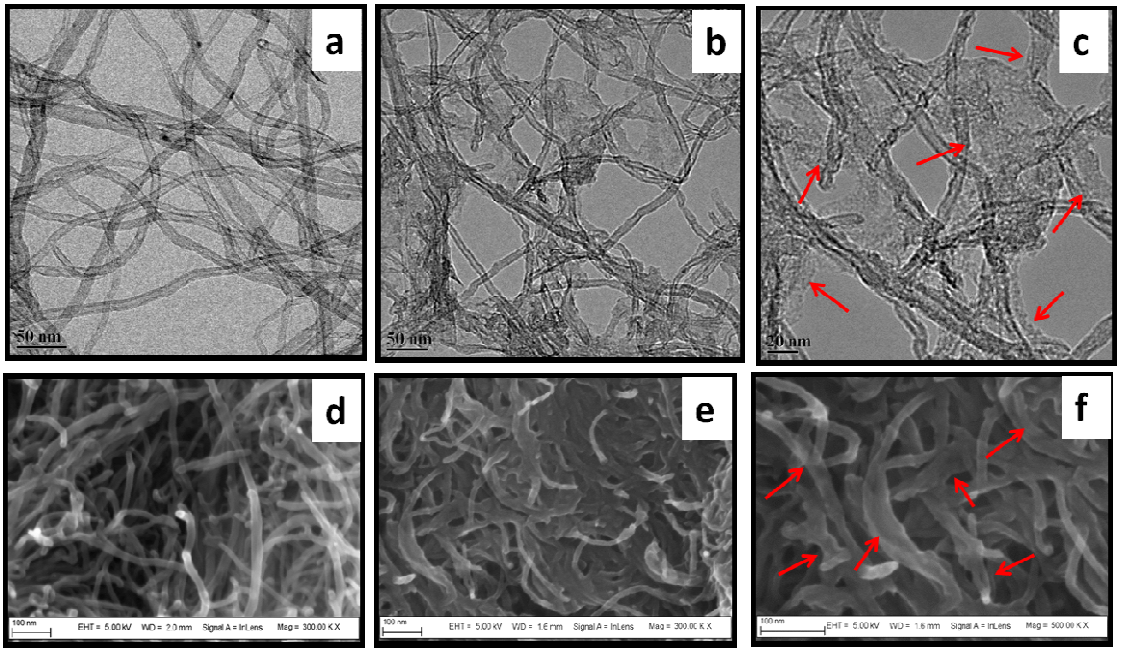

Figure 2: TEM and SEM images of MWCNTs (a, d) and UZ-MWCNTs (b, c, e & f)

Raman spectroscopic analysis is by far the most important technique for carbon nanotubes characterization. G-band corresponds to planar vibration of sp^2 hybridized carbon atoms of ordered graphitic structures of MWCNTs, while D-band corresponds to the structural defects associated with the respective MWCNTs (Figure 3). Raman spectra of pristine MWCNTs and partially UZ-MWCNTs are shown in Figure 3. MWCNTs show D and G-band at ~1346 and 1583 cm^{-1} respectively, while UZ-MWCNTs exhibit D and G-band at ~1351 and 1598 cm^{-1} respectively. The intensity ratio of D band to G-band (I_D/I_G) increases slightly from 1.01 to 1.10 for UZ-MWCNTs, which indicates that unzipping process may increase the defects in MWCNTs. It is reported that the I_D/I_G ratio of the UZ-MWCNTs may not increase significantly due to unzipping, if the pristine MWCNTs exhibit high I_D/I_G ratio due to higher extent of defects associated with it [28].

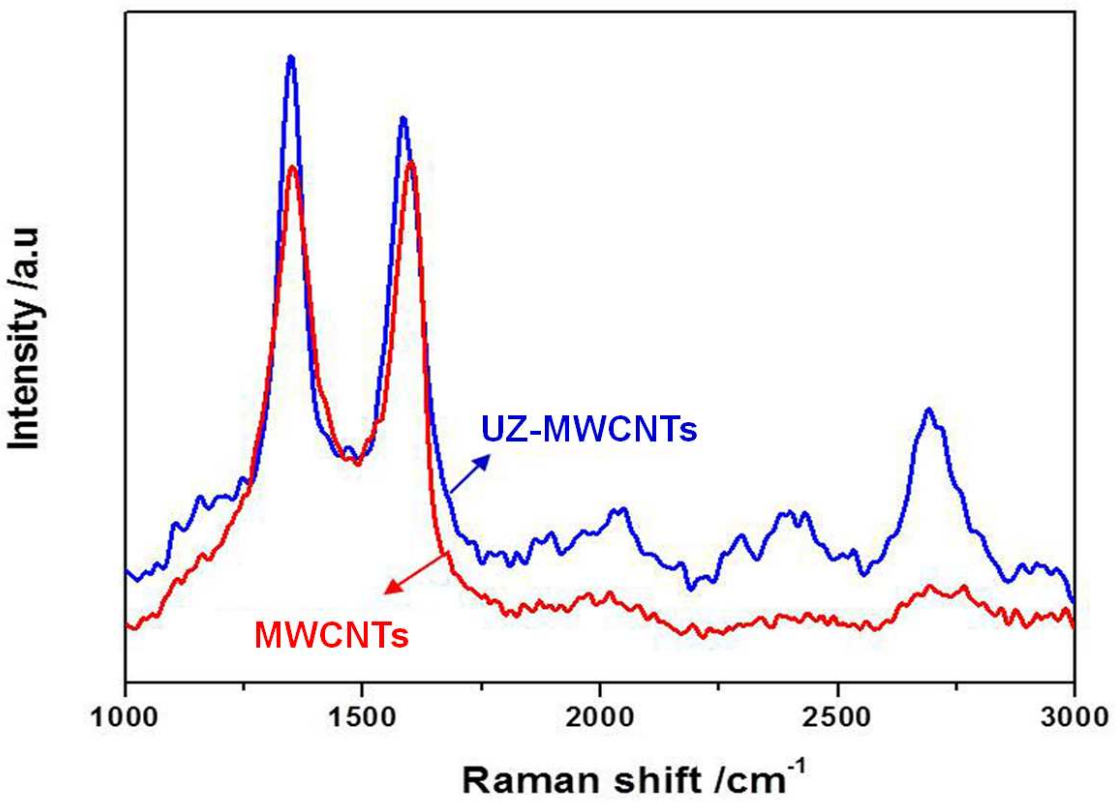

Figure 3: Raman spectra of pristine MWCNTs and UZ-MWCNTs

XRD analysis was carried out to investigate the structural changes due to the partial unzipping of MWCNTs. XRD patterns of MWCNTs and UZ-MWCNTs are depicted in Figure 4. Pristine MWCNTs exhibit a strong peak at 2θ=25.9° corresponding to the *d*-spacing of 3.42 Å. UZ-MWCNTs exhibit a comparatively broad peak corresponding to 2θ=25.1° corresponding to the d-spacing of 3.55 Å. The broad peak corresponding to UZ–MWCNTs and subsequent increase in d-spacing indicate the disrupted arrangement of unzipped layers of MWCNTs. In addition to this, a small peak at 2θ=23.0° corresponding to interlayer d-spacing of about 3.86 Å is also noticed, which may be due to the existence of some of the layers of MWCNTs, which are unzipped to a larger extent or fully opened layers of MWCNTs.

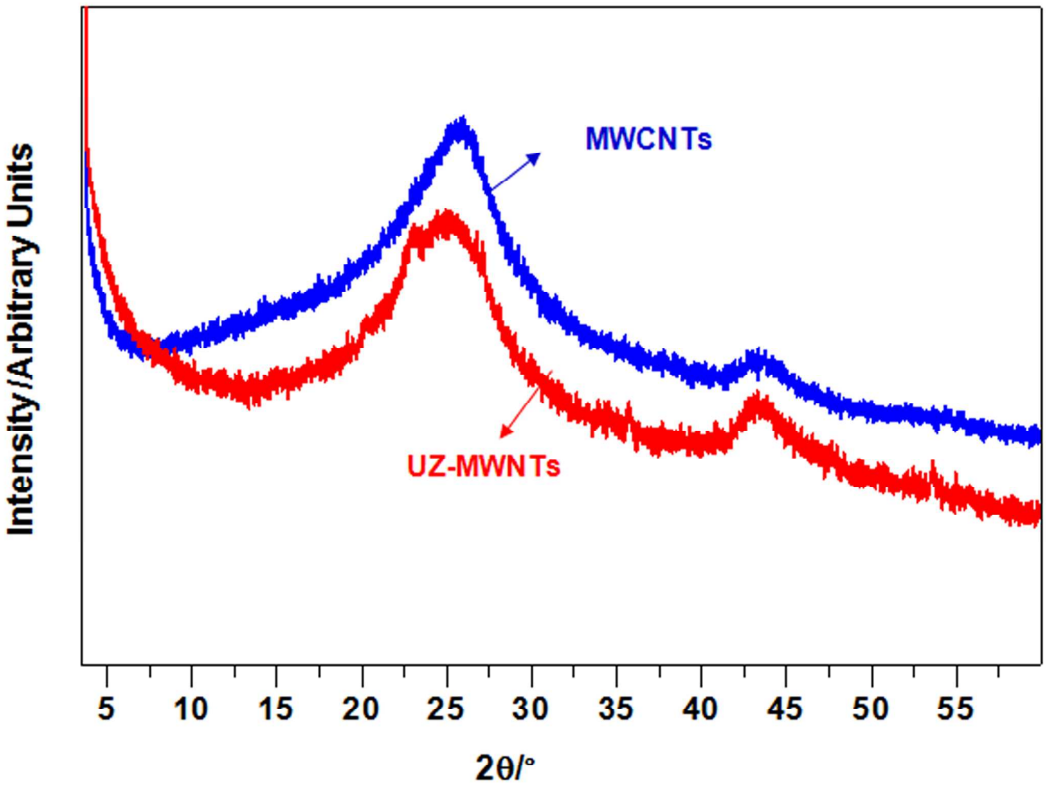

Figure 4: XRD pattern of MWCNTs and UZ-MWCNTs

3.2 Electrochemical studies

Reduced UZ-MWCNTs have been used in the fabrication of unit cell. Chemical reduction of oxidized MWCNTs with hydrazine was carried out in order to restore the electrical conductivity of UZ-MWCNTs, which is close to that of pristine MWCNTs [25]. Figure 5 shows the CV profile of UZ-MWCNTs and pristine MWCNTs based supercapacitors at the scan rate of 25 mVs^{-1}. Even though both MWCNTs and UZ-MWCNTs based supercapacitors exhibit rectangular shaped CV profile, the shape of the CV profile associated with UZ-MWCNTs based supercapacitor is slightly distorted as compared to that of pristine MWCNTs based supercapacitor. Typically an ideal capacitor exhibits perfect rectangular shaped CV profile. The shape of the CV profile indicates the quality of the capacitive behavior. It may be commented that electric double layer capacitance contribution

plays a dominant role with negligible pseudo-capacitance contribution as no peak could be observed in connection with pseudo-capacitance behaviour.

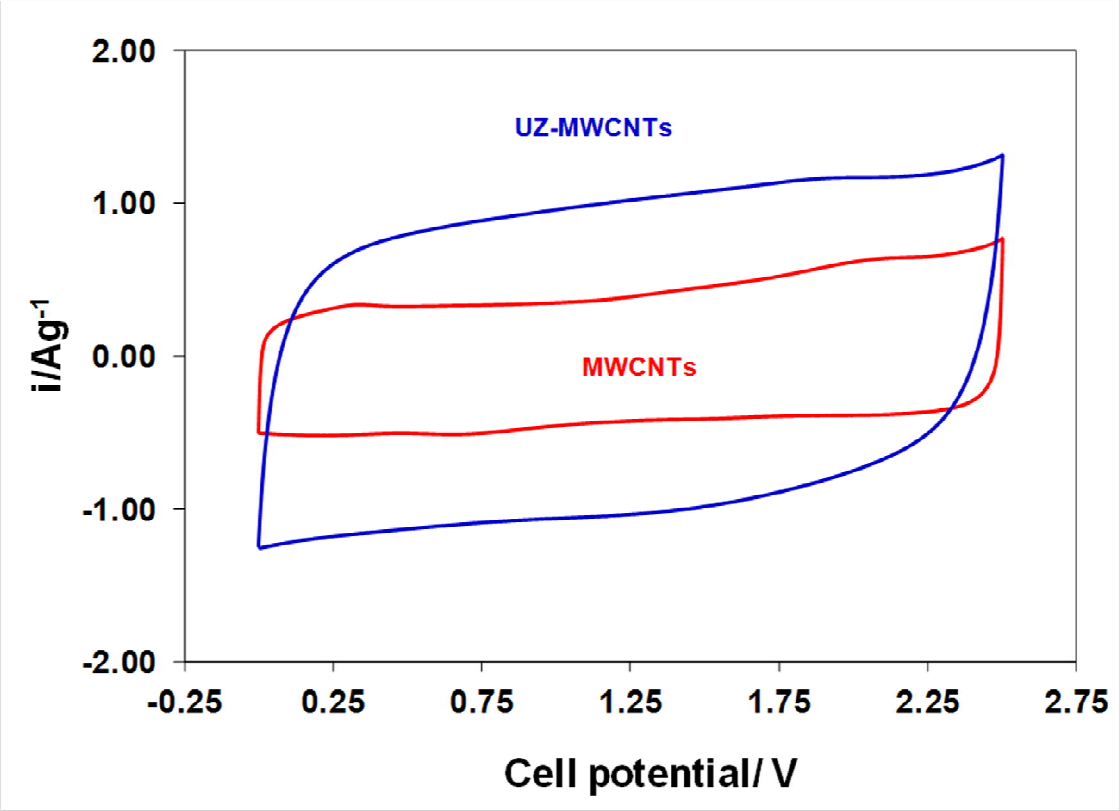

Figure 5: CV profile of UZ-MWCNTs and MWCNTs based supercapacitors

It may also be observed from the CV profile that the specific capacitance of UZ-MWCNTs based supercapacitor is higher than pristine MWCNTs based supercapacitor. Specific capacitance (*SC*) for the total active material in both the electrodes of the supercapacitor unit cell has been calculated using equation 1:

$$SC = \frac{Q_a + Q_c}{2ms} \quad (1)$$

where, Q_a and Q_c are the integrated values of anodic and cathodic charges respectively, *m* is the total active mass in the both electrodes and *s* is the scan rate. The capacitance value

obtained has been multiplied by 4 to evaluate the specific capacitance of the single electrode [36]. The specific capacitance of UZ-MWCNTs and pristine MWCNTs was found to be ~41.2 and ~22.3 Fg^{-1} respectively. The observed increase in the specific capacitance may be due to the partial unzipping of MWCNTs, which increases the specific surface area of UZ-MWCNTs. Figure S1 depicts the nitrogen adsorption/desorption isotherm of MWCNTs and UZ-MWCNTs. MWCNTs and UZ-MWCNTs show specific surface area of ~230 and ~355 $m^2 g^{-1}$ respectively.

The faster at which the supercapacitor changes its polarity of the current when the potential of the scan is reversed, is a measure of internal resistance of the cell [37]. CV profile exhibits that pristine MWCNTs based supercapacitor changes the polarity faster than UZ-MWCNTs. This indicates that pristine MWCNTs based supercapacitor exhibits lower internal resistance than UZ-MWCNTs based supercapacitor. This is attributed to the disruption of the flow of electrons due to the unzipping in UZ-MWCNTs. Consequently, the internal resistance of UZ-MWCNTs based supercapacitor increases and also results in distorted rectangle shaped CV profile as compared to pristine MWCNTs based supercapacitor. The observed results are in agreement with that reported by Saghafi et al. for aqueous electrolyte [28].

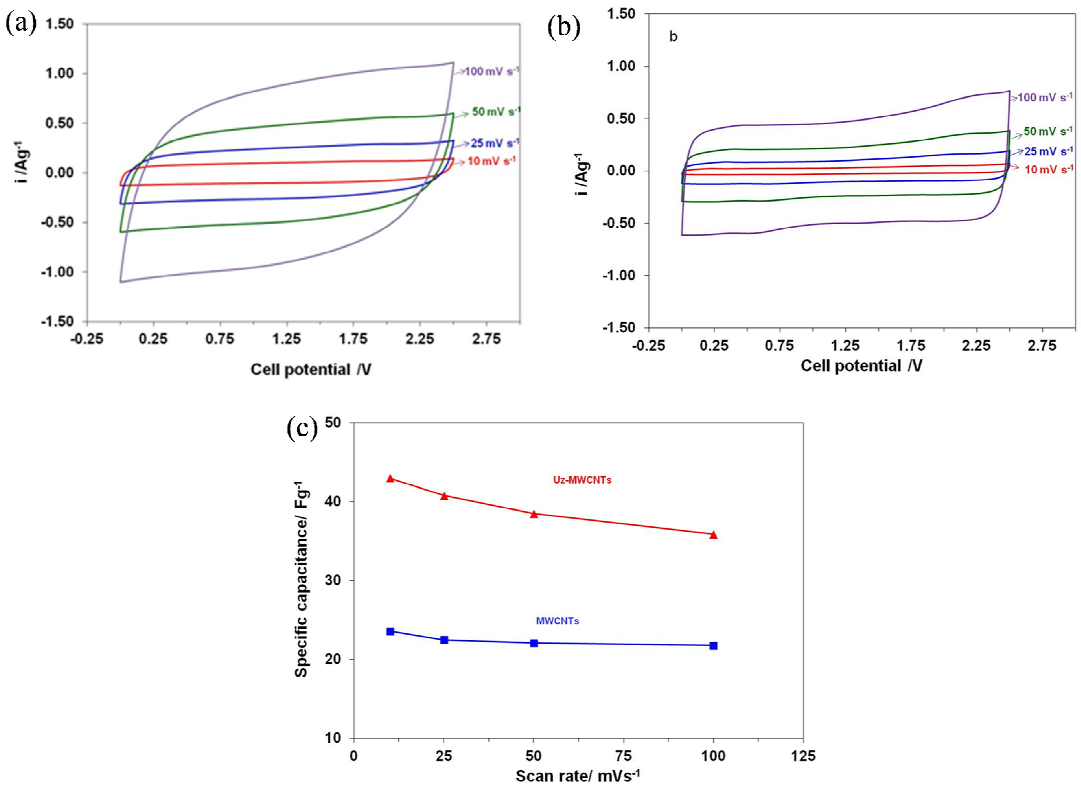

Figure 6: CV profile of UZ-MWCNTs based supercapacitor (a) and pristine MWCNTs based supercapacitor (b) at different scan rates; (c) Specific capacitance of UZ-MWCNTs and MWCNTs based supercapacitors as a function of scan rate

Figure 6a and 6b show the CV profile of UZ-MWCNTs and pristine MWCNTs based supercapacitors at different scan rates while Figure 6c depicts the decrease in specific capacitance as a function of increasing scan rates. With increase in the scan rate, the distortion in the CV profile of UZ-MWCNTs based supercapacitor is more evident as compared to that of pristine MWCNTs based supercapacitor. The specific capacitance dependence on the scan rate is observed to be different between UZ-MWCNTs and pristine MWCNTs based supercapacitor. In case of UZ-MWCNTs based supercapacitor, specific capacitance decreases monotonically as a function of increasing scan rate, while for pristine MWCNTs based supercapacitor, it remains almost unchanged. The observed results may be attributed to the following phenomenon. UZ-MWCNTs exhibit large structural defects due to

the opening of layers and hence, probability of diffusion of ions through the unzipped opening to the inner tubes increases with increase in the scan rate. Moreover, at higher scan rate, the concentration gradient at the 'electrode/electrolytes interface' is expected to be more, which may induce a lag in anodic and cathodic current response that may in turn distort the CV profile [34]. Further, when this is coupled with higher internal resistance of the cell, the distortion effect is more pronounced at higher scan rates. In case of pristine MWCNTs based supercapacitor, the 'charge-discharge' behavior is largely a surface phenomenon even though small amount of ions may even penetrate through the open ends of the MWCNTs [8, 21, 39]. Additionally, pristine MWCNTs based supercapacitor exhibits lesser internal resistance. Hence, a marginal change in specific capacitance is observed and the corresponding CV profile does not change significantly with increasing scan rate.

Galvanostatic 'charge-discharge' cycles have been carried out for UZ-MWCNTs and pristine MWCNTs based supercapacitors at different current densities. Figure 7 exhibits the 'charge-discharge' profile for UZ-MWCNTs and pristine MWCNTs based supercapacitors at different current densities. It shows that UZ-MWCNTs based supercapacitor exhibits large IR drop due to large internal resistance, which increases with increase in the current density. However, pristine MWCNTs based supercapacitor does not exhibit appreciable IR drop in the current density range studied. Generally, all practical supercapacitor shows both resistive and capacitive component in it. During application, a large amount of current may flow through the supercapacitor, which may lead to a considerable amount of voltage loss due to the internal resistance of the cell. This loss is parasitic and it should be minimized as much as possible even though it cannot be eliminated fully [37].

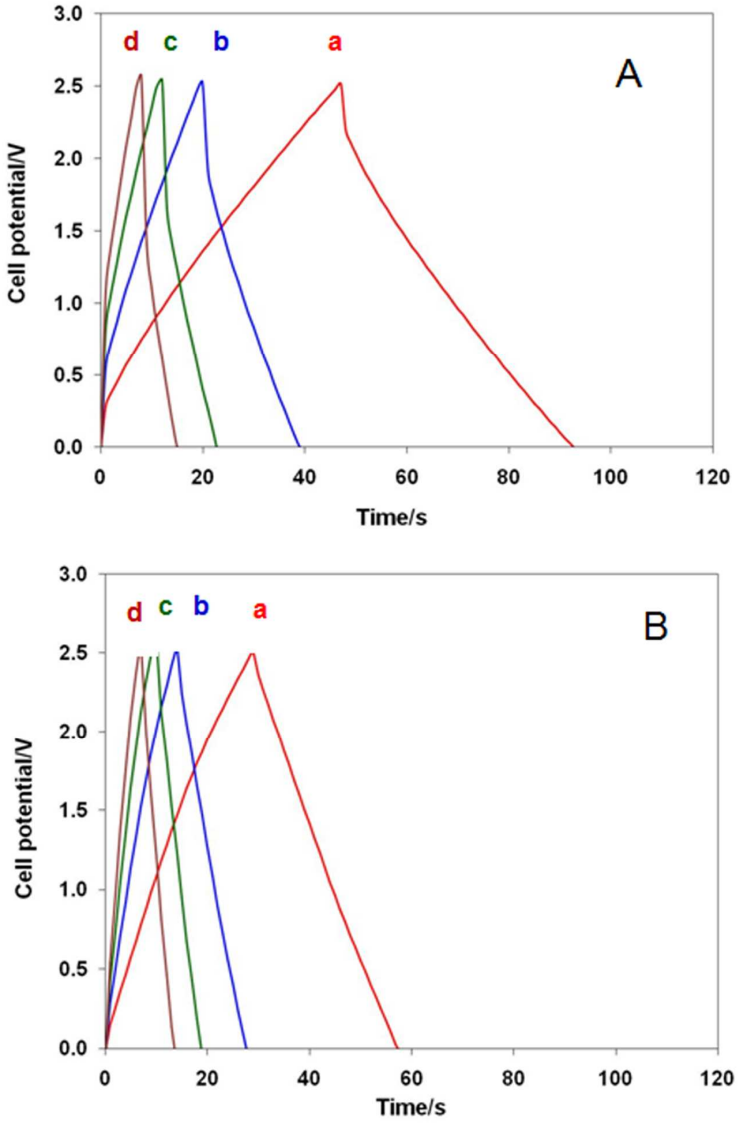

Figure 7: 'Charge-discharge' profile for UZ-MWCNTs (A) and pristine MWCNTs (B) based supercapacitors at current densities of a) 0.5 Ag^{-1}, b) 1.0 Ag^{-1} c) 1.5 Ag^{-1} and d) 2.0 Ag^{-1}

The specific capacitance (*SC*) of the electrode material was calculated using the eqn. 2;

$$SC = \frac{It}{Vm} \qquad (2)$$

where, I is the current, t is time of discharge, V is the potential difference and m is the total active mass in both the electrodes of the supercapacitor. The specific energy (E_{sp}) of the electrode material was calculated using eqn. 3;

$$E_{sp} = \frac{0.5(SC)V_{\max}{}^{2}}{3.6} \quad (3)$$

where, V_{max} is the maximum voltage of the supercapacitor. Table 1 provides the specific capacitance and specific energy of UZ-MWCNTs and pristine MWCNTs based supercapacitor at different current densities. The specific capacitance decreases with increase in current density, which is found to be similar to that observed for specific capacitance dependence on the scan rate. The specific energy of UZ-MWCNTs based supercapacitor is higher than reported in Ref. [28]. A comparison of the specific capacitance of unzipped MWCNTs based supercapacitor by various methods reported in the literature is provided in Table 2. One of the important aspects on which the specific capacitance of UZ-MWCNTs based supercapacitor depends is the type of electrolyte used in the supercapacitor. For instance, Wang et al. reported a specific capacitance of UZ-MWCNTs based supercapacitor as 265, 180 and 95 Fg^{-1} in electrolyte containing 6 M KOH, 1 M H_2SO_4 and 1 M Na_2SO_4 respectively and the enhancement in the specific capacitance over pristine MWCNTs based supercapacitor was reported to be 8.0, 7.2 and 7.9 times in the respective electrolytes [27]. Similarly, Silva et al. demonstrated ~2 times improvement in the specific capacitance of UZ-MWCNTs based supercapacitor in 1 M H_2SO_4 [28]. In the present study, the enhancement in the specific capacitance of UZ-MWCNTs in 1 M $TEABF_4$ in PC is observed to be ~2 times higher than that of pristine MWCNTs based supercapacitor. Further, the improvement in the specific capacitance of UZ-MWCNTs based supercapacitor also depends on the ionic

conductivity of the electrolyte, diffusivity of ions into the pore of UZ-MWCNTs, method of unzipping and the specific surface area.

Table 1: Specific capacitance and specific energy of UZ-MWCNTs and MWCNTs based supercapacitor at different current density

Current density (Ag^{-1})	UZ-MWCNTs		MWCNTs	
	SC (Fg^{-1})	E_{sp} (kW kg^{-1})	SC (Fg^{-1})	E_{sp} (kW kg^{-1})
0.5	42,8	35.8	23.6	20.5
1.0	39.1	33.9	22.3	19.4
1.5	36.9	32.0	22.1	19.1
2.0	35.4	30.7	21.8	18.9

Table 2: Summary of the specific capacitance reported for MWCNTs and UZ-MWCNTs based supercapacitor

Method of unzipping	**Electrolyte**	**Sp. Capacitance (Fg^{-1})**		**Reference**
		MWCNTs	**UZ-MWCNTs**	
Tour method	3M NaOH	11.8	165	[26]
Hummer method	6M KOH	33	265	[27]
Hummer method	1M H_2SO_4	25	180	[27]
Hummer method	1M Na_2SO_4	12	95	[27]
Tour method	0.5 M KCl	8	62	[28]
Tour method	1 M H_2SO_4	25	50	[29]
Modified Tour method	6M KOH	25	106	[30]
Tour method	1 M $TEABF_4$ in PC	22.2	42.8	This study

In order to study the performance of UZ-MWCNTs and MWCNTs based supercapacitors at elevated temperatures, electrochemical studies were carried out at different temperatures. Propylene carbonate (PC) has been used as the supporting electrolyte in the supercapacitor cells as it has the potential to withstand temperature much higher than 100 °C

without any degradation [14]. The CV profile of UZ-MWCNTs and MWCNTs based supercapacitors at various temperatures is depicted in Figure 8. UZ-MWCNTs based supercapacitor exhibits an enhanced current response as a function of increasing temperature. The increase in the anodic and cathodic current indicates that specific capacitance increases with increase in temperature. Specific capacitance calculated for UZ-MWCNTs and pristine MWCNTs based supercapacitors at different temperatures are shown in Table 3. At elevated temperatures, the probability of the dissociation of ion pairs may increase. Hence, the concentration of ions at the vicinity of the 'electrode/electrolytes interface' may also increase, which may result in an enhanced and compact electric double layer formation. The enhancement in specific capacitance with increase in temperature is higher for UZ-MWCNTs based supercapacitor as compared to pristine MWCNTs based supercapacitor. UZ-MWCNTs possess unzipped tubes with openings ranging from one atomic to fully unzipped CNTs [25]. With increase in temperature, kinetic energy associated with the ions in the electrolytes may increase and may diffuse into the openings of the innermost tubes of UZ-MWCNTs. This may further increase the accessible area of UZ-MWCNTs and may result in an increased electric double layer formation. However, in case of pristine MWCNTs based supercapacitor, diffusion of ions into the inner tubes is restricted even though some amount of ions may diffuse into inner canals through the openings of the tips of MWCNTs [8, 39]. Hence, the enhancement of specific capacitance with increase in temperature for UZ-MWCNTs based supercapacitor is much higher as compared to pure MWCNTs based one.

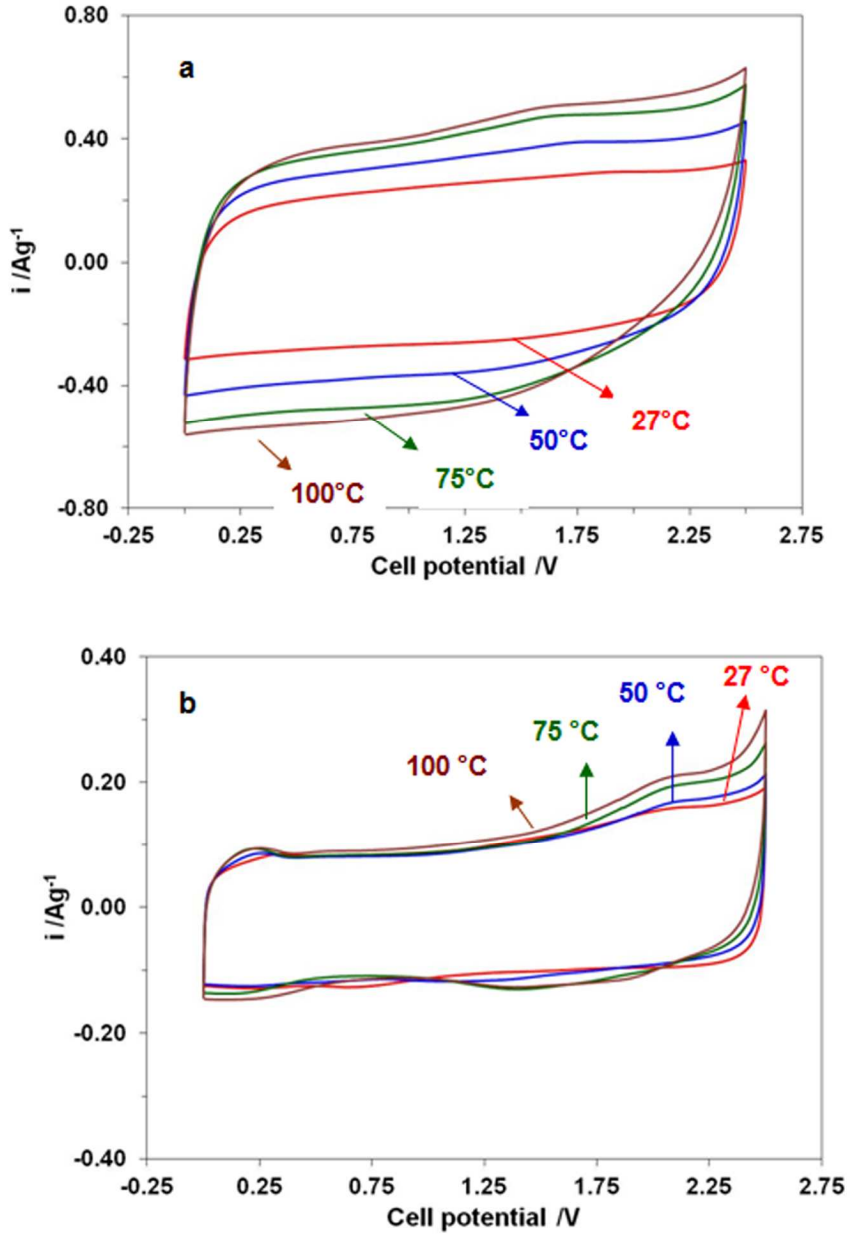

Figure 8: CV profile of UZ-MWCNTs based supercapacitor (a) and pristine MWCNTs based supercapacitor (b) at different temperatures

Further, it is reported that at elevated temperature, physio-sorption of electrolyte ions may take place at the surface of MWCNTs, which may lead to the pseudo-capacitance [14, 35]. The resultant pseudo-capacitance also contributes to the overall increase in specific capacitance along with the double layer capacitance. Generally, the presence of pseudo-

capacitance behavior appears as a hump in the CV profile due to the redox reaction. It may be noticed from Figure 8 that any appreciable hump is not observed for UZ-MWCNTs based supercapacitor, which indicates that pseudocapacitance contribution is negligible. However, small humps are noticed for CVs corresponding to pristine MWCNTs based supercapacitor at higher temperature, which indicates the contribution of pseudocapacitance in a smaller extent.

Table 3: Specific capacitance of the pristine MWCNTs and UZ-MWCNTs based supercapacitors at different temperature

Temperature (°C)	UZ-MWCNTs		MWCNTs	
	SC_{cv} (Fg^{-1})	SC_{cd} (Fg^{-1})	SC_{cv} (Fg^{-1})	SC_{cd} (Fg^{-1})
27	41.2	42.8	21.5	22.2
50	56.1	58.8	23.1	25.1
75	69.2	70.2	24.4	26.4
100	73.9	74.8	25.7	27.7

SC_{cv} - specific capacitance obtained from CV profile at a scan rate of 25 mV s^{-1}

SC_{cd} - specific capacitance obtained from charge-discharge cycle at a current density of 0.5 Ag^{-1}

The galvanostatic 'charge-discharge' profile for UZ-MWCNTs and pristine MWCNTs based supercapacitors at elevated temperatures is depicted in Figure 9. The specific capacitance calculated from the discharge curve at different temperatures is provided in Table 3. The effect of temperature on the specific capacitance corresponding to various supercapacitors based on CNTs reported in the literature is provided in Table 4. In the present context, it is important to note that the specific capacitance of UZ-MWCNTs based

supercapacitor is ~3 times higher as compared to that of pristine MWCNTs based supercapacitor at 100 °C.

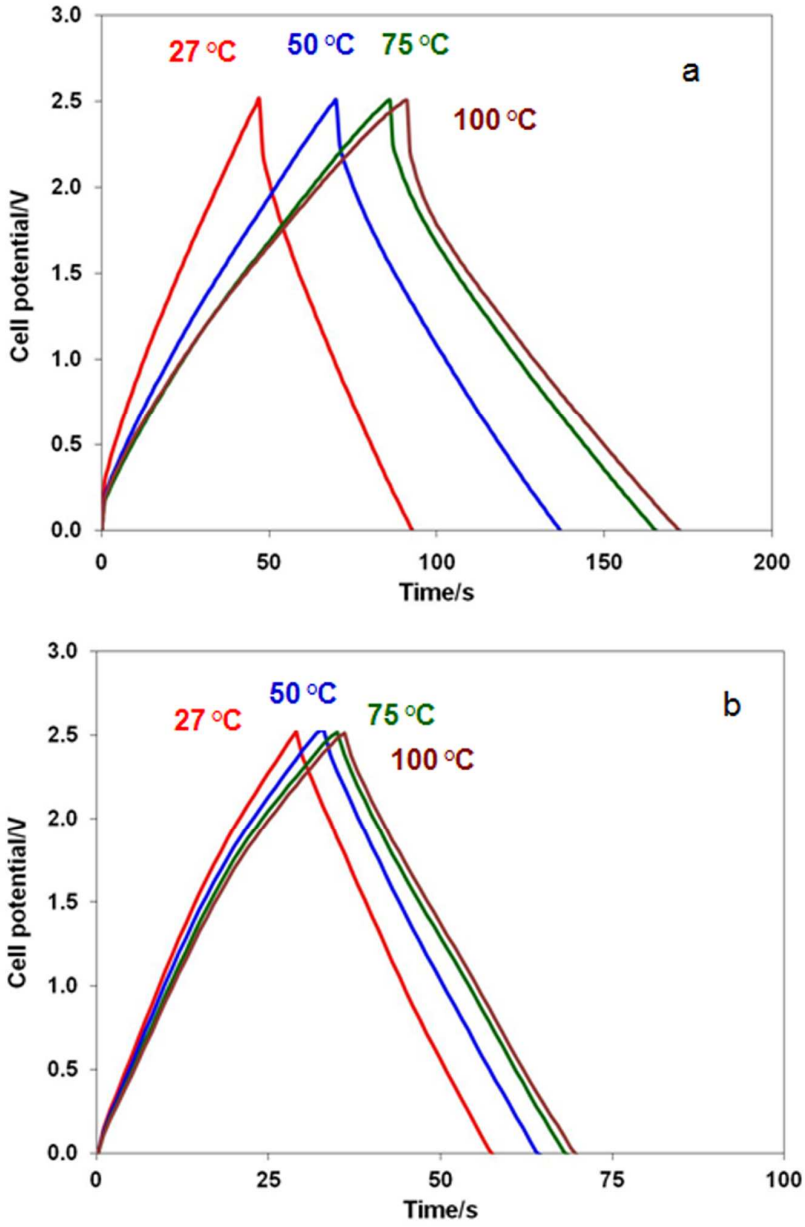

Figure 9: 'Charge-discharge' profile of UZ-MWCNTs (a) and MWCNTs (b) based supercapacitors at different temperatures

In order to study the resistive and capacitive components of the supercapacitors at different temperatures, electrochemical impedance spectroscopic analysis has been carried

out. Generally, Nyquist plot of a supercapacitor exhibits a 'semi-circle' feature at very high frequency followed by a slanting line at mid frequency range and a vertical line at very low frequency. The intercept at the x axis of the spectrum at high frequency end represents the solution resistance (R_s) of the electrolytes. The 'semi-circle' feature represents the parallel combination of interfacial capacitance (C_i) and charge transfer resistance (R_c). The mid-frequency slanting line, which is due to diffusion resistance, represents the Warbarg resistance (W). The vertical line at very low frequency, which is generally parallel to Z″ axis represents the mass capacitance (C_m). However, if vertical line is inclined toward Z′ axis, then it represents the cumulative effect of C_m with leakage resistance (R_l) in parallel combination.

Table 4: Comparison of specific capacitance (SC) of CNTs based various supercapacitor reported at 27 °C and 100 °C

Electrode Material	**Electrolytes**	**SC at 27 °C (Fg^{-1})**	**SC at 100 °C (Fg^{-1})**	**Ref.**
SWCNTs	1M $TEABF_4$ in PC	23.4*	31.7	[14]
MWCNTs	H_3PO_4 doped poly(2,5 benzimidazole)	28.8	52.7	[39]
MWCNTs	1M $TEABF_4$ in PC	22.2	27.7	This study
UZ-MWCNT	1M $TEABF_4$ in PC	42.8	74.8	This study

* SC at 25 °C

Nyquist plot of UZ-MWCNTs based supercapacitor at different temperatures is shown in Figure 10a. Nyquist plot can be represented by Randle equivalent circuit and the circuit elements are illustrated in Figure 10b. The best fit values are provided in Table 5. It may be noticed that the solution resistance of the supercapacitor decreases with increase in temperature. The enhanced dissociation and mobility of the ions may increase the ionic

conductivity of the electrolytes, which in turn decrease the solution resistance with increase in temperature.

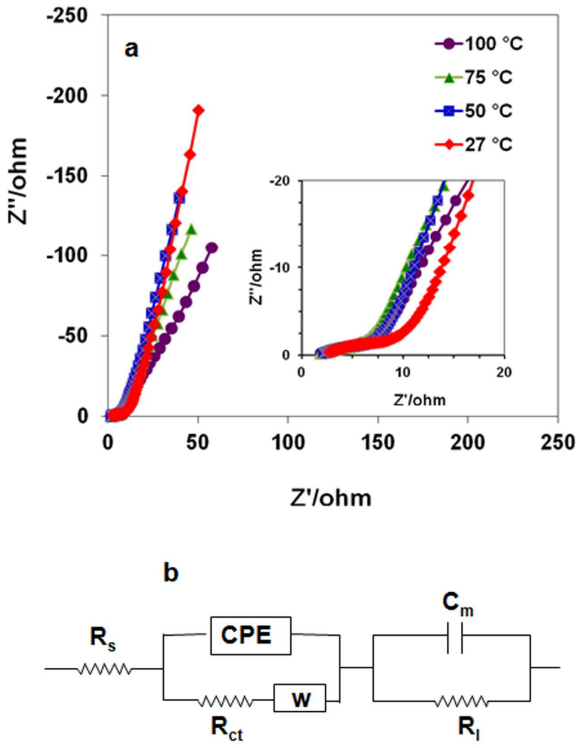

Figure 10: Impedance spectroscopy of UZ-MWCNTs based supercapacitor; Inset shows the plot at high frequency end; b) Equivalent circuit for impedance spectra of UZ-MWCNTs based supercapacitor

Table 5: Fitting parameters of the equivalent circuit for UZ-MWCNTs based supercapacitor

Temperature (°C)	R_s (Ω)	CPE		R_{ct} (Ω)	W (Ω)	R_l (kΩ)	C_m (F g^{-1})
		C_i (mF g^{-1})	n				
27	2.29	2.82	0.35	8.71	8.30	1.82	37.8
50	1.74	4.26	0.34	6.26	6.48	1.35	53.1
75	1.42	6.14	0.32	4.67	5.17	0.58	65.0
100	1.48	8.21	0.38	4.55	8.23	0.23	68.9

The plot shows a depressed semi-circle feature at very high frequency and it is represented by constant phase element (CPE). C_i represents the interfacial capacitance between the current collector and the electrode material and it is increased with increase in temperature. The exponent '*n*' indicates the non-ideal behavior of the capacitance with values ranging between 0 and 1 [40]. It is reported that exponent '*n*' is related to the surface roughness of the electrode material [41]. The low value of '*n*' may be attributed to large surface roughness due to unzipped MWCNTs and the value does not change much with increase in temperature. It is observed that R_{ct} decreases with increase in temperature and this may be attributed to enhanced charge transfer between the active electrode materials and the electrode to current collector. Warburg resistance is decreased with increase in temperature followed by a rise at 100 °C. This behavior may be attributed to the facilitated diffusion of ions to inner most layers of UZ-MWCNTs through the openings of the tubes due to increased kinetic energy at elevated temperature. As expected, the mass capacitance increases with increase in temperature due to enhanced electric double layer formation. It is also noticed (Figure 10a) that vertical lines of the plot deviate significantly from Z" axis with increase in temperature. This suggests that the leakage resistance decreases with increase in temperature, which may be attributed to the undesirable side reactions. With increase in temperature, the rate of side reaction may increase, which in turn may decrease the leakage resistance R_l.

Figure 11a and 11b show the Nyquist plot at different temperatures and Randle equivalent circuit of the plot for pristine MWCNTs based supercapacitor, respectively. The best fit values of the equivalent circuit are shown in Table 6. CPE and R_{ct} elements in the equivalent circuit are eliminated, since pristine MWCNTs based supercapacitor exhibits negligible C_i and R_{ct} values at all the temperatures due to higher electrical conductivity of pure MWCNTs. It can be seen from the vertical spike at the mid-frequency region of Nyquist

plot (inset in Figure 11a) that the Warburg resistance is lower than that observed for UZ-MWCNTs based supercapacitor. In case of pristine MWCNTs based supercapacitor, as mentioned earlier, most of the capacitance is due to electric double layer formation at the outer surface of MWCNTs even though small amount pseudo-capacitance behaviour co-exists. Hence, the Warburg resistance should be negligible at all temperatures unlike that of UZ-MWCNTs based supercapacitor. The increase in the mass capacitance with increase in temperature is very less. Pristine MWCNTs based supercapacitor exhibits a higher leakage resistance as compared to UZ-MWCNTs based supercapacitor, which may be attributed to lesser side reactions. Hence, the deviation of the vertical line away from the Z″ axis is lesser for pristine MWCNTs based supercapacitors at higher temperatures.

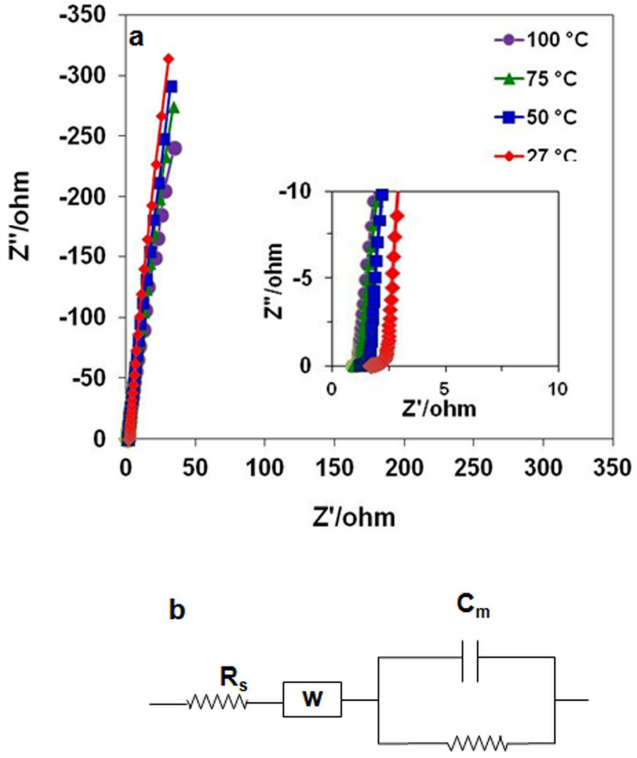

Figure 11: a) Impedance spectroscopy of pristine MWCNTs based supercapacitor at different temperatures and b) Equivalent circuit for impedance spectra of pristine MWCNTs based supercapacitor

Table 6: Fitting parameters of the equivalent circuit for pristine MWCNTs based supercapacitor

Temperature (°C)	R_s (Ω)	W (Ω)	R_l (kΩ)	C_m (F g^{-1})
27	1.65	1.52	3.86	22.2
50	1.16	1.12	2.18	23.9
75	0.91	0.87	1.77	25.2
100	0.85	0.78	0.99	25.8

Frequency dependant impedance is defined as:

$$Z(\omega) = Z'(\omega) + iZ''(\omega) \quad (4)$$

where, Z' and Z'' are real and complex part of the impedance respectively. Similarly the frequency dependant capacitance can be resolved into real and complex capacitance as

$$C(\omega) = C'(\omega) - iC''(\omega) \quad (5)$$

where,

$$C' = \frac{-Z''(\omega)}{\omega|Z(\omega)|^2} \quad (6)$$

$$C'' = \frac{Z'(\omega)}{\omega|Z(\omega)|^2} \quad (7)$$

C′ and C″ is the real and loss capacitance respectively [42, 43]. C′ corresponds to the capacitance measured by galvanostatic 'charge-discharge' measurement or CV method. C″ represents energy loss due to irreversible process that leads to hysteresis for example, dielectric loss of the medium. The real and loss capacitance of UZ-MWCNTs and MWCNTs based supercapacitors are shown in Figure 12 and 13 respectively.

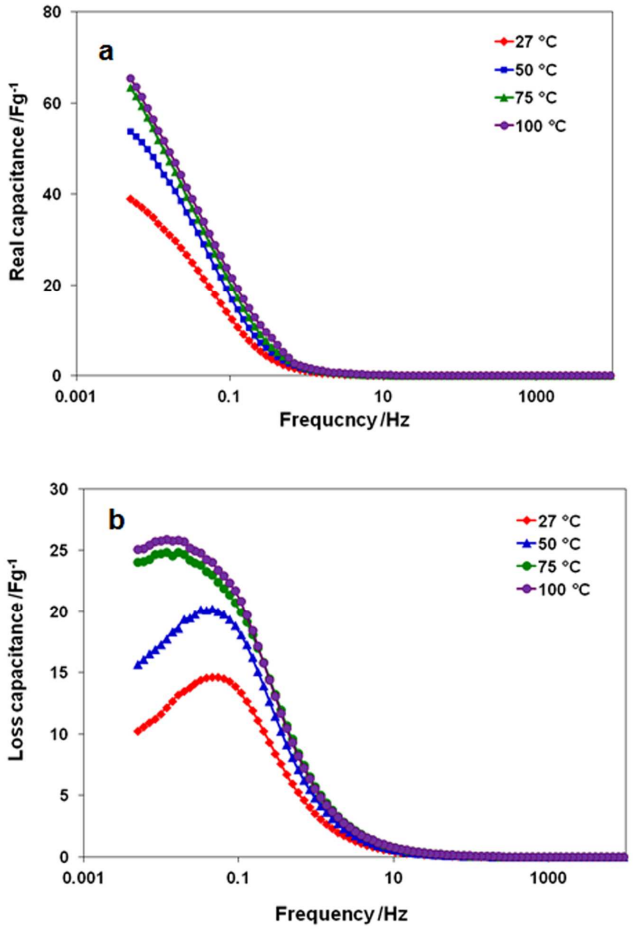

Figure 12: Real (a) and loss (b) capacitance of UZ-MWCNTs based supercapacitor

The real capacitance increases with increase in temperature, which is consistent with the values obtained from the impedance spectroscopic analysis. The loss capacitance also increases with increase in temperature, which may be due to an increase in dielectric loss with increase in temperature. The peak of loss capacitance represents a frequency f_0, and the

time constant (τ_0) is defined by $1/f_0$. The time constant represents the dielectric relaxation time and corresponds to figure of merit of a supercapacitor [44]. At time constant τ_0, the phase angle of the supercapacitor is 45°. In other words, the time below which the supercapacitor behaviour is resistive and above which it depicts capacitive behaviour.

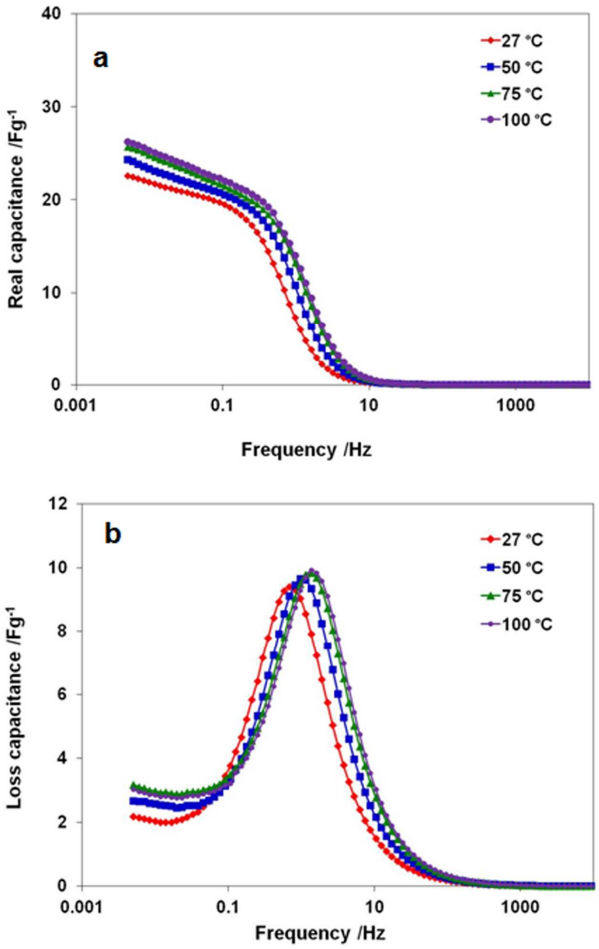

Figure 13: Real (a) and loss (b) capacitance of pristine MWCNTs based supercapacitor

The time constant of the respective supercapacitor is shown in Table 7. Quite anomalously, it is found that in spite of increase in temperature, the time constant has increased for UZ-MWCNTs based supercapacitor. The results indicate clearly that the defect in the UZ-MWCNTs based electrode largely increases the resistance of the supercapacitor and it delays the charging process. Moreover, the diffusion of ions at inner most layers takes

longer time, which manifests in larger time constant. In addition to this, parasitic side reactions at elevated temperatures may also delay the charging process. This effect can be clearly seen from the impedance plot where the vertical spike deviates from the Z″-axis at high temperature. In case of the CV plot of UZ-MWCNTs based supercapacitor (Figure 8a), the delay in the current polarity change when the direction of scan is reversed at high voltage end, which is also due to the large parasitic reactions. The time constant corresponding to pristine MWCNTs based supercapacitor show a decreasing trend with increase in temperature as expected. The results indicate that charging process is facilitated during heating of pristine MWCNTs based supercapacitor. Smaller time constant indicates the higher rate capability of the pristine MWCNTs based supercapacitor.

Table 7: Time constant for UZ-MWCNTs and pristine MWCNTs based supercapacitors at different temperatures

Temperature (°C)	τ_0 for UZ-MWCNTs (s)	τ_0 for MWCNTs (s)
27	26.1	1.55
50	26.1	1.03
75	72.2	0.74
100	72.2	0.68

Continuous ‘charge-discharge’ cycling was carried out for the supercapacitors at constant current of 2.5 mA cm^{-2}. Cyclic protocol of 1000 cycles at room temperature followed by 500 cycles at 100 °C and subsequent 500 cycles at room temperature was followed. The variation in specific capacitance of UZ-MWCNTs and pristine MWCNTs based supercapacitors is shown in Figure 14.

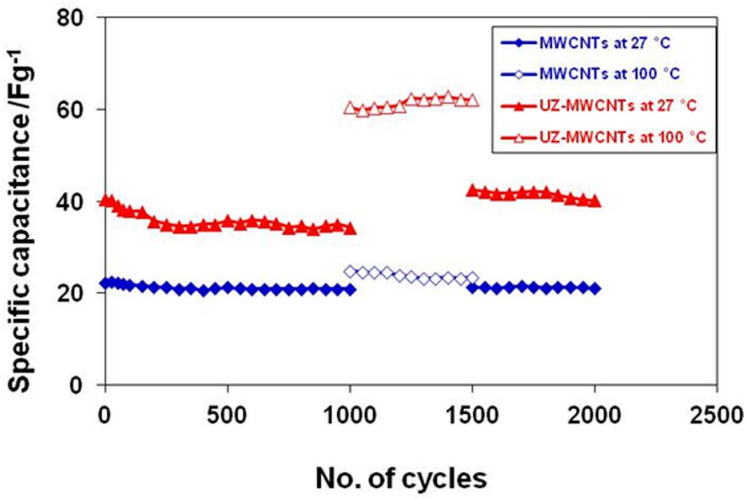

Figure 14: Continuous 'charge-discharge' cycling of UZ-MWCNTs and pristine MWCNTs based supercapacitors

During initial room temperature cycling, UZ-MWCNTs based supercapacitor indicates a sharp decrease in specific capacitance for initial 200 cycles and thereafter specific capacitance reaches almost a plateau. Once the cycling temperature of supercapacitor is increased to 100 °C, specific capacitance increases to higher values as expected. During subsequent room temperature cycling, UZ-MWCNTs based supercapacitor exhibits higher specific capacitance as compared to the specific capacitance observed at room temperature cycling during first 1000 cycles. It is expected that some of the ions, which may diffuse into the inner tubes at higher temperature might be retained in the vicinity of inner most tubes even after the temperature is lowered. Hence, during subsequent room temperature cycling, the accessible surface area available to the ions may be higher than that initial room temperature cycling. A similar kind of phenomenon at high temperature cycling has been reported earlier in the literature [39, 45]. Pristine MWCNTs based supercapacitor shows almost constant specific capacitance during the initial 'charge-discharge' cycling at room temperature. Similarly, during high temperature cycling, supercapacitor exhibits higher capacitance than that observed at room temperature. Subsequent room temperature cycling

also depicts almost constant specific capacitance close to that of initial room temperature cycling.

Conclusions

Longitudinal unzipping of MWCNTs was carried out by chemical method. Partially unzipped MWCNTs could be assessed via TEM, XRD and Raman spectroscopic analyses. A comparative study between UZ-MWCNTs based supercapacitor and pristine MWCNTs based supercapacitor showed that UZ-MWCNTs based supercapacitor exhibited a specific capacitance of 42.8 Fg^{-1}, whereas pristine MWCNTs exhibited a specific capacitance of 22.2 Fg^{-1}. Unzipping of MWCNTs could increase the surface area from 230 m^2g^{-1} to 355 m^2g^{-1}, which might be responsible for the increase in the specific capacitance of UZ-MWCNTs based supercapacitor. The specific energy of UZ-MWCNTs and MWCNTs was found to be 35.8 and 20.5 $kWkg^{-1}$ respectively, at a current density 0.5 Ag^{-1}. Electrochemical performance of both UZ-MWCNTs and pristine MWCNTs based supercapacitors at elevated temperature were also evaluated. The specific capacitance of UZ-MWCNTs was observed to be ~3 times higher as that of pristine MWCNTs at 100 °C. Impedance spectroscopic analysis showed that resistance associated during charging process was higher for UZ-MWCNTs based supercapacitor than MWCNTs based supercapacitor. The impedance spectra of the supercapacitors were resolved into real and loss capacitance. Both real and loss capacitance were increased with increase in temperature. The time constant of the UZ-MWCNTs based supercapacitor increased from 26.1 s to 72.2 s when the temperature was increased from 27 °C to 100 °C. However, for pristine MWCNTs based supercapacitor, it decreased from 1.55 s to 0.68 s when the temperature was increased from 27 °C to 100 °C. Continuous 'charge-discharge' cycling study of UZ-MWCNTs based supercapacitor showed an initial decrease in specific capacitance, which subsequently stabilized to a constant value. It exhibited higher

specific capacitance at elevated temperature and during subsequent room temperature cycling it exhibited higher specific capacitance than that of initial room temperature cycling. Pristine MWCNTs based supercapacitor showed negligible increase in specific capacitance with increase in temperature during continuous 'charge-discharge' cycles.

In brief, it can be concluded that Uz-MWCNTs based supercapacitor (table S1) can be utilized effectively for high temperature application using non-aqueous electrolytes.

Acknowledgements

The authors would like to acknowledge SAIF and CRNTS facility at IIT Bombay for carrying out TEM and Raman spectroscopic analysis.

References

1 B. E. Conway, *Electrochemical Supercapacitors, Scientific Fundamentals and Technological Applications*, Kluwer Academic/ Plenum Publishers, New York, USA, 1999.

2 A. Burke, *J. Power Sources*, 2000, **91**, 37.

3 K. Kotz, M. Carlen, *Electrochim. Acta*, 2000, **45**, 2483.

4 P. Simon, Y. Gogotsi, *Nat. Mater.*, 2008, **7**, 845.

5 G. Wang, L. Zhang, J. Zhang, *Chem. Soc. Rev.*, 2012, **41**, 797.

6 G. Lota, K. Fic, E. Frackowiak, *Energy Environ. Sci.,* 2011, **4**, 1592.

7 L. L. Zhang, X. S. Zhano, *Chem. Soc. Rev.*, 2009, **38**, 2520.

8 E. Frackowiak, F. Beguin, *Carbon*, 2002, **40**, 1775.

9 E. Frackowaick, M. Metenier, V. Bertagna and F. Beguin, *Appl. Phys. Lett.*, 2000, **77,** 2421.

10 C. Emmenegger, P. Mauron, P. Sudan, P. Wenger, V. Herman, R. Gallay, A. Zuttel, *J. Power Sources*, 2003, **124,** 321.

11 M. Jung, H. G. Kim, J. K. Lee, O. S. Joo, S. Mho, *Electrochim. Acta*, 2004, **50,** 857.

12 D. Futaba, K. Hata, T. Yamada, T. Hiraoka, Y. Hayamizu, Y. Kakudate , O. Tanaike, H. Hatori, M. Yumura and S. IIjima, *Nat. Mater.*, 2006, **5**, 987.

13 J. Y. Lee, K. Hyeok, J. K. Heo, Y. H. Lee, *J. Phys. Chem. B*, 2003, **107** 8812.

14 C. Masarau, H. F. Zeng, K. H. Hung, B. Wei, *ACS Nano*, 2009, **3**, 2199.

15 X. Li, J. Rong and B. Wei, *ACS Nano*, 2010, **4**, 6039.

16 Z. Niu, W. Zhou, J. Chen, G. Feng, H. Li, W. Ma, J. Li, H. Dong, Y. Ren, D. Zhao, S. Xie, *Energy Environ. Sci.*, 2011, **4**, 1440.

17 S. W. Lee, B. S. Kim, S. Chen, Y. S. Hom, P. T. Hammond, *J. Am. Chem. Soc.*, 2009, **131**, 671.

18 E. Frackowiak, K. Jurewicz, S. Delpeux, F. Beguin, *J. Power Sources*, 2001, **97-98**, 822.

19 S. Wen, S. Mho, I. H. Yeo, *J. Power Sources*, 2006, **163,** 304.

20 K. Jurewicz , K. Babel. R. Pietrzak, S. Delpeux, H. Wachowska, *Carbon*, 2006, **44**, 2368.

21 J. S. Ye, X. Liu, H. F. Cui, W. D. Zhang, F. S. Sheu, T. M. Lim, *Electrochem. Commun.*, 2005, **7**, 249.

22 Y. T. Kim, Y. Ito, K. Tadai, T. Mitani, U. S. Kim, H. S. Kim and B. W. Cho, *Appl. Phys. Lett.,* 2005, **87,** 234106.

23 Y. T. Kim, T. Mitani, *J. Power Sources*, 2006, **158**, 1517.

24 B. J. Yoon, S. H. Jeong, K. H. Lee, H. S. Kim, C. G. Park, J. H. Han, *Chem. Phys. Lett.*, 2004, **388**, 170.

25 D. V. Kosynkin, A. L. Higginbotham, A. Sinitskii, Y. R. Lomeda, A. Dimiev, B. K. Price, J. M. Tour, *Nature*, 2009, **458**, 872.

26 G. Wang, Y. Ling, F. Qian, X. Yang, X. X. Liu, Y. Li, *J. Power Sources*, 2011, **196**, 5209.

27 H. Wang, Y. Wang, Z. Hu, X. Wang, *ACS Appl. Mater. Interfaces*, 2012, **4**, 6827.

28 M. Saghafi, F. Mahboubi, S. Mohajerzadeh, M. Fathi, R. Holze, *Curr. Appl. Phys.*, 2014, **14,** 1335.

29 R. C- Silva, A. M- Gomez, S. V- Diaz, F. T- Lopez, A. L. Elias, N. P- Lopez, H. Muramatsu, T. Hayashi, K. Fujisawa, Y. A. Kim, M. Endo and M. Terrones, *ACS Nano*, 2013, **7**, 2193.

30 C. Zhang, Z. Peng, J. Lin, Y. Zhu, G. Ruan, C-C. Hwang, W. Lu, R. H. Hauge and J. M. Tour, *ACS Nano*, 2013, **7**, 5151.

31 D. B. Shinde, J. Debgupta, A. Kushwaha, M. Aslam, V. K. Pillai, *J. Am. Chem. Soc.*, 2011, **133**, 4166.

32 D. D. Potphode, P. Sivaraman, S. P. Mishra, M. Patri, Electrochim. Acta, 2015, **155**, 402.

33 W. E. Mahmoud, F S. Al-Hazmi, GH. Al-Harbi, Chem. Engg. J., 2015, **281**,192.

34 X. Li, T. Li, Q, Zhong, X. Zhang, H. Li, J. Huang, Mater. Lett., 2014, **180**, 132.

35 X. Li, T. Li, Q. Zhong, K. Du, H. Li, J. Huang, Electrochim. Acta, 2014, **125**, 170.

36 D. Qu, H. Shi, *J. Power Sources*, 1998, **74**, 99.

37 F. Lufrano, P. Staiti, *Electrochim. Acta*, 2004, **49**, 2683.

38 34 D. Antiohos, G. Folkes, P. Sherrell, S. Ashraf, G. G. Wallace, P. Aitchison, A. T. Harris, J. Chen, A. I. Minett, *J. Mater. Chem.*, 2011, **21**, 15987.

39 R. S. Hastak, P. Sivaraman, D. D. Potphode, K. Shashidhara, A. B. Samui, *J. Solid State Electrochem.*, 2012, **16**, 3215.

40 C. Portet, P. L. Taberna, P. Simon, C. L. Robert, *Electrochim. Acta*, 2004, **49**, 905.

41 W. C. Chen, T. C. Wen, H. Teng, *Electrochim. Acta*, 2003, **48**, 641.

42 P. L. Taberna, P. Simon, J. F. Fauvarque, *J. Electrochem. Soc.*, 2003, **150**, A292.

43 C. Portet, P. L. Taberna, P. Simon, E. Flahaut, C. L. Robert, *Electrochim. Acta*, 2005, **50**, 4174.

44 J. Miller, in *Proceedings of the 8th International Seminar in Double-Layer Capacitors and Similar Energy Storage Devices*, Deerfield Beach, FL, Dec. 7-9, 1998.

45 R. S. Hastak, P. Sivaraman, D. D. Potphode, K. Shashidhara, A. B. Samui, *Electrochim. Acta*, 2012, **59**, 296.

Supporting Nomenclature of the symbols used in the text (SN1)

CNTs	Carbon nanotubes (CNTs)
MWCNTs	Multi-walled carbon nanotubes (MWCNTs)
SWCNTs	Single-walled carbon nanotubes (SWCNTs)
UZ-MWCNTs	Unzipped multi-walled carbon nanotubes (UZ-MWCNTs)
PC	Propylene carbonate (PC)
$TEABF_4$	Tetra ethylene ammonium tetrafluoroborate ($TEABF_4$)
Q_a	Anodic charge
Q_c	Cathodic charge
S	Scan rate
T	Discharge time
M	Active electrode mass
SC	Specific capacitance
SC_{cv}	Specific capacitance obtained from CV profile
SC_{cd}	Specific capacitance obtained from charge-discharge cycle
E_{sp}	Specific energy
I	Current
V	Voltage
V_{max}	Maximum voltage of the supercapacitor
R_s	Solution resistance
R_c	Charge transfer resistance
W	Warbarg resistance
C_i	Interfacial capacitance
C_m	Mass capacitance
R_l	Leakage resistance
CPE	Constant phase element

ω	Angular frequency
$Z(\omega)$	Frequency dependant impedance
$Z'(\omega)$	Frequency dependant real part of impedance
$Z''(\omega)$	Frequency dependant imaginary part of impedance
$C(\omega)$	Frequency dependant capacitance
$C'(\omega)$	Frequency dependant real capacitance
$C''(\omega)$	Frequency dependant loss capacitance
τ	Time constant

Supporting Figure 1

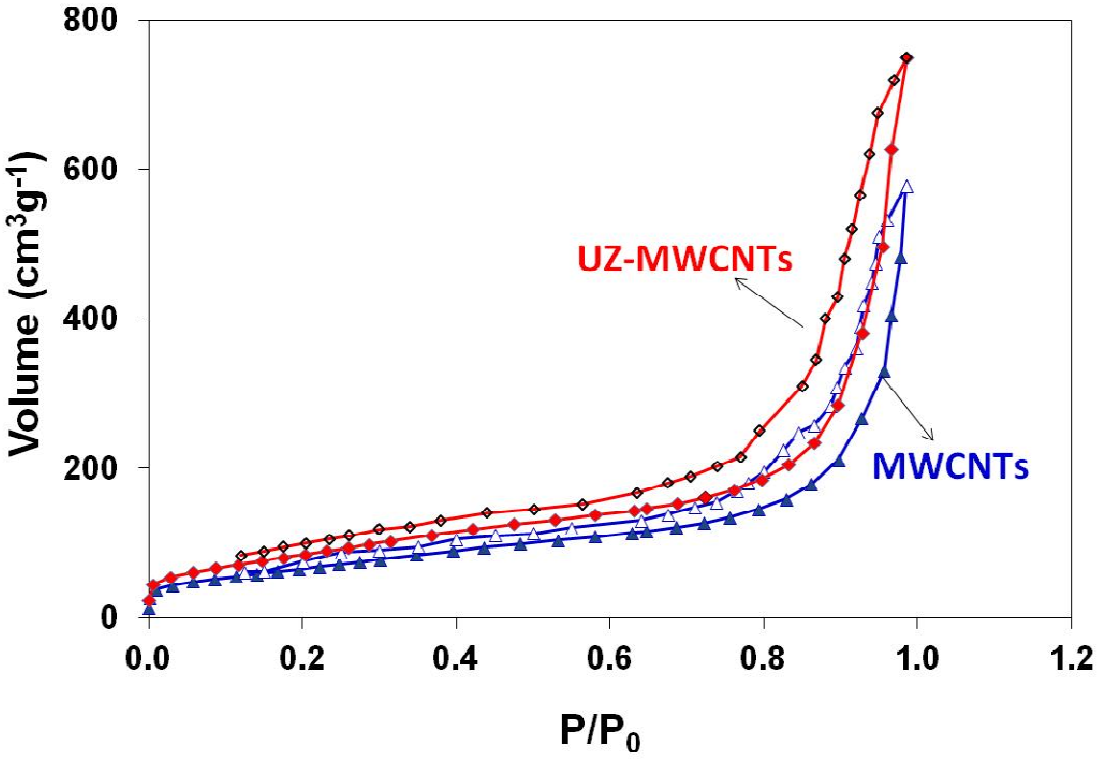

Figure S1: Nitrogen adsorption/desorption isotherm of MWCNTs and UZ-MWCNTs

Table S1: Comparison of some important properties of MWCNTs and UZ-MWCNTs

Properties	**MWCNTs**	**UZ-MWCNTs**
BET surface area (m^2g^{-1})	230	355
Specific capacitance (SC_{cd}) at 27 °C (F g^{-1})	22.2	42.8
Specific capacitance (SC_{cd}) at 100 °C (F g^{-1})	27.7	74.8
Specific energy (E_{sp})of the supercapacitor ($kWkg^{-1}$)	20.5	35.8
Time constant (τ_0) of the supercapacitor at 27 °C (s)	1.55	26,1
Time constant (τ_0) of the supercapacitor at 100 °C (s)	0.68	72.2